THE SHAPES AND SURFACE FEATURES OF PROMETHEUS AND PANDORA

PHILIP J. STOOKE

Department of Geography, University of Western Ontario, London, Ontario, Canada

(Received 17 November 1992)

Abstract. Topographic models of Saturn's F-Ring shepherd satellites Prometheus and Pandora were derived from the shapes of limbs and terminators in Voyager images, modified locally to accommodate large craters and ridges. The models are presented here in tabular and graphic form, including the first published maps of the satellites. The shape of Prometheus is approximated by a triaxial ellipsoid with axes of 145, 85 and 60 km. The volume is estimated to be $3.9 \pm 1.0 \times 10^5$ km^3, significantly smaller than previous estimates. A system of prominent ridges and valleys cross the north polar region. Prometheus appears to be less heavily cratered than the other small satellites near the edge of the rings, though this may be an artifact of the low resolution of available images. Pandora is approximated by a triaxial ellipsoid with axes of 114, 84 and 62 km. The volume is estimated to be $3.1 \pm 1.0 \times 10^5$ km^3. Its surface appears to be very heavily cratered.

Introduction

Prometheus and Pandora, the F-Ring shepherd satellites of Saturn, were observed by the cameras of Voyagers 1 and 2 in 1980 and 1981 respectively (Smith *et al.*, 1981, 1982). Only the Voyager 2 images show any details of the shape and surface features. Despite severe limitations of resolution and coverage the images were used to create rough topographic models and maps of each satellite. Prometheus has approximate dimensions of 145 by 85 by 65 km. The images reveal a number of ridges and valleys on the northern side of the satellite. Several craters roughly 20 km in diameter are visible, and a few possible craters down to the resolution limit of about 10 km, but the surface generally appears smoother and less heavily cratered than that of the nearby satellites Pandora, Janus and Epimetheus. Pandora is roughly 114 by 84 by 62 km in size and appears to be very heavily cratered. No features on either satellite have been given names by the International Astronomical Union.

This is the fourth in a series of reports on the topography of non-spherical worlds. The previous three studies were of the nucleus of Halley's Comet (Stooke and Abergel, 1991), the jovian satellite Amalthea (Stooke, 1992a) and Saturn's co-orbital satellite Epimetheus (Stooke, 1993).

Data

The Voyager 2 images of Prometheus and Pandora used for this study are listed in Table I. Those used for mapping are identified by an asterisk in the first column. The remaining images were too smeared to be useful, but are listed in Table I for

Earth, Moon, and Planets **62**: 199–221, 1993.

TABLE I

Voyager images of Prometheus and Pandora

FDS number	Spacecraft lat.	Spacecraft long.	Sub-solar lat.	Sub-solar long.	Phase angle	Scale (km/pixel)
Prometheus						
43975.27*	19	184	8	202	20	11.0
43975.31	19	184	8	202	20	11.0
43975.35*	19	184	8	202	20	11.0
43975.39	19	184	8	202	20	11.0
43989.26*	30	65	8	99	38	6.7
43998.29*	30	270	8	295	30	3.4
Pandora						
43982.59	21	187	8	205	24	8.2
43983.05	21	188	8	206	24	8.2
43983.11*	21	190	8	208	24	8.2
43983.17	21	191	8	209	24	8.2
43998.15*	26	75	8	144	67	3.8
44004.56*	31	80	8	273	139	7.5

* Images used for shape modelling and mapping.

completeness. Images are identified by FDS (Flight Data Subsystem) number. They were obtained on Planetary Data System (PDS) CD-ROMs (or magnetic tape where not yet available on CD-ROM) from NASA's National Space Science Data Center.

Latitudes and longitudes given in this paper are planetocentric. The quoted latitudes assume a rotation axis perpendicular to the orbit plane, and the quoted longitudes assume synchronous rotation. The prime meridian of each satellite faces Saturn and longitudes increase opposite to the direction of rotation, following planetary cartographic conventions. The Voyager images are too few in number and too low in resolution to confirm these assumptions, but the positions of the long axes of the satellites in the various images are consistent with them. The rotation states could be confirmed given a small number of images from the Cassini spacecraft at resolutions of 3 km/pixel. Repetitive imaging at resolutions around 1 km/pixel could be used to characterize librations.

Voyager 2 obtained four images (FDS 43975.27 to 43975.39) at long range which show Prometheus in transit across the disk of Saturn. Two are too smeared to be useful. The remaining two, with fewer than ten pixels across the disk, are difficult to interpret but show distinct irregularities in shading. Image 43989.26 has a resolution of 6.7 km per pixel and shows only larger topographic features, but it provides the only coverage of most of the leading side (centred on longitude 90°). The best image, 43998.29, covers most of the trailing side at 3.4 km per pixel and a phase angle of 30°. Given the large differences in viewing angle and resolution, no stereoscopic viewing is possible. The south polar region is beyond the limb in all Voyager images.

Pandora was observed in one multispectral sequence of four images (43982.59

to 43983.17) with a resolution of 8.2 km/pixel, giving about 10 pixels across the disk. Despite the low resolution a crater near the northern limb is faintly visible, and extensive processing suggests the presence of two other depressions, though these latter features are doubtful. FDS 43998.15 is the most useful of the Pandora images, revealing several large craters on the leading side. FDS 44004.46 is a narrow crescent view obtained by the wide-angle camera at 7.5 km/pixel. An accompanying narrow angle frame would have given the highest resolution of any image of the smaller satellites of Saturn, but it was lost due to the instrument platform malfunction near closest approach to Saturn. Parts of the shaded surface of Pandora are made faintly visible by light reflected from Saturn in the latter two images, providing a little more information on the shape of the satellite.

Method

The shapes of Prometheus and Pandora were modelled from limb and terminator shapes in the images identified with an asterisk in Table I, using the technique described by Stooke and Keller (1990), Stooke and Abergel (1991) and Stooke (1992a). Limb and terminator positions were digitized from the images. Initial triaxial ellipsoid models of each satellite were created using the axis dimensions (140 by 100 by 75 km for Prometheus, 110 by 85 by 65 km for Pandora) given by Thomas *et al.* (1983). The models were viewed and illuminated in the orientations given in Table I and registered to the outlines digitized from the images. They were reshaped until they duplicated the limbs and terminators in the images. Figure 1 shows the positions of limb and terminator traces on the two models. Areas where several traces converge (e.g., around the equatorial region of Prometheus) are modelled most reliably, whereas regions not crossed by a limb or terminator (e.g., the south polar region of each satellite) are least reliable. Some attempt was made at this stage to model features, particularly ridges and craters, which appear on the images but are not seen on a limb or terminator. Contours in these regions are merely suggestive of the local topography.

The limbs are probably located to within about one pixel in the plane of the image, and the terminators to within about two pixels. Uncertainties are caused by smearing, aliasing effects at the limb, and low signal levels near the terminators. When the limbs are transferred to a body-fixed coordinate system for mapping, their locations may be uncertain by up to several tens of degrees perpendicular to the limb traces of Figure 1, reducing reliability in the model to no better than about twice the single pixel resolution of the original image even in the best areas.

Relative elevations near terminators may be more accurate since small variations in topography produce large changes in the shape of the terminator. Absolute radii near terminators are reasonably reliable only near limb traces, within the limits outlined above. Despite these considerable uncertainties, the models derived by these techniques are the best yet available since the low resolution and minimal overlap between images preclude stereoscopic imaging and control point triangu-

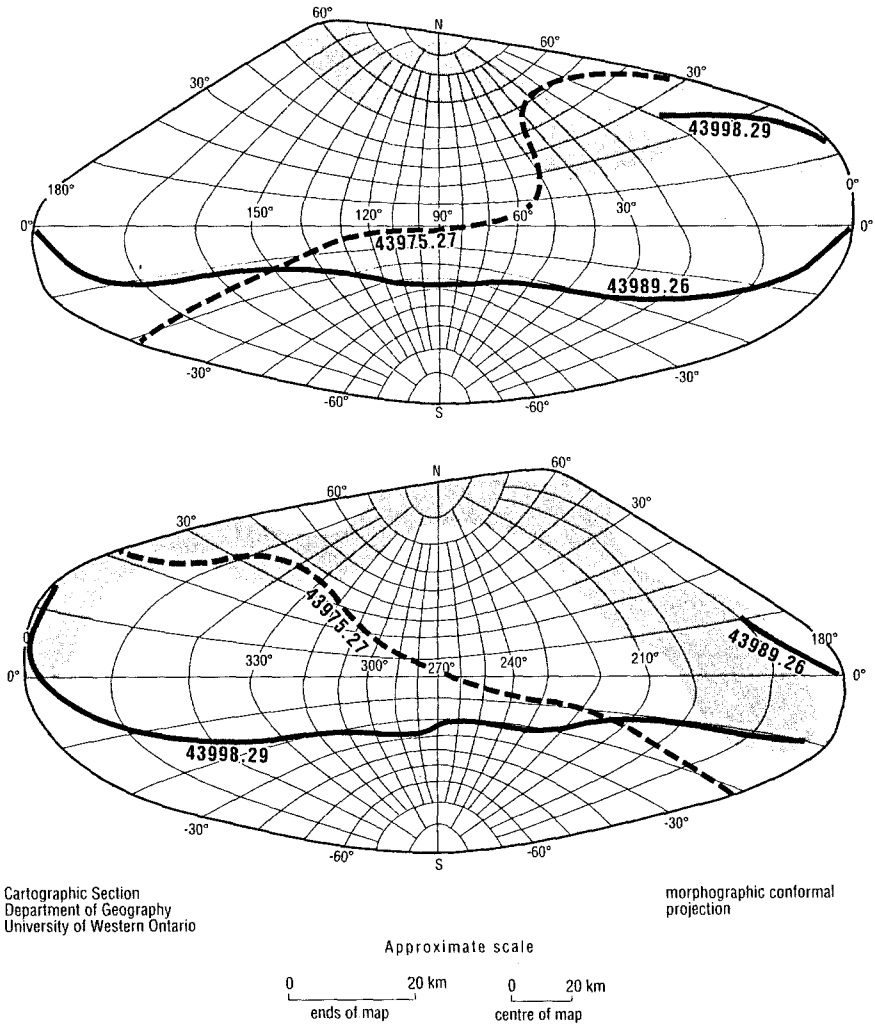

Fig. 1. (a) Locations on Prometheus of the limbs (solid lines) and terminators (shaded areas) used to derive the shape model. The map projection is the same as that used in Figures 4 to 6. (b) Locations on Pandora of the limbs (solid lines) and terminators (shaded areas) used to derive the shape model. The map projection is the same as that used in Figures 7 to 9.

lation. The radius matrices for the two models at the 5° spacing used during modelling may be obtained from the author on diskette.

The Shape of Prometheus

The topographic model of Prometheus is given in Table II and illustrated in Figures 2 to 7. Latitude-longitude grids corresponding to three Voyager views are given in Figure 2. The rotation axes are vertical in these views regardless of the

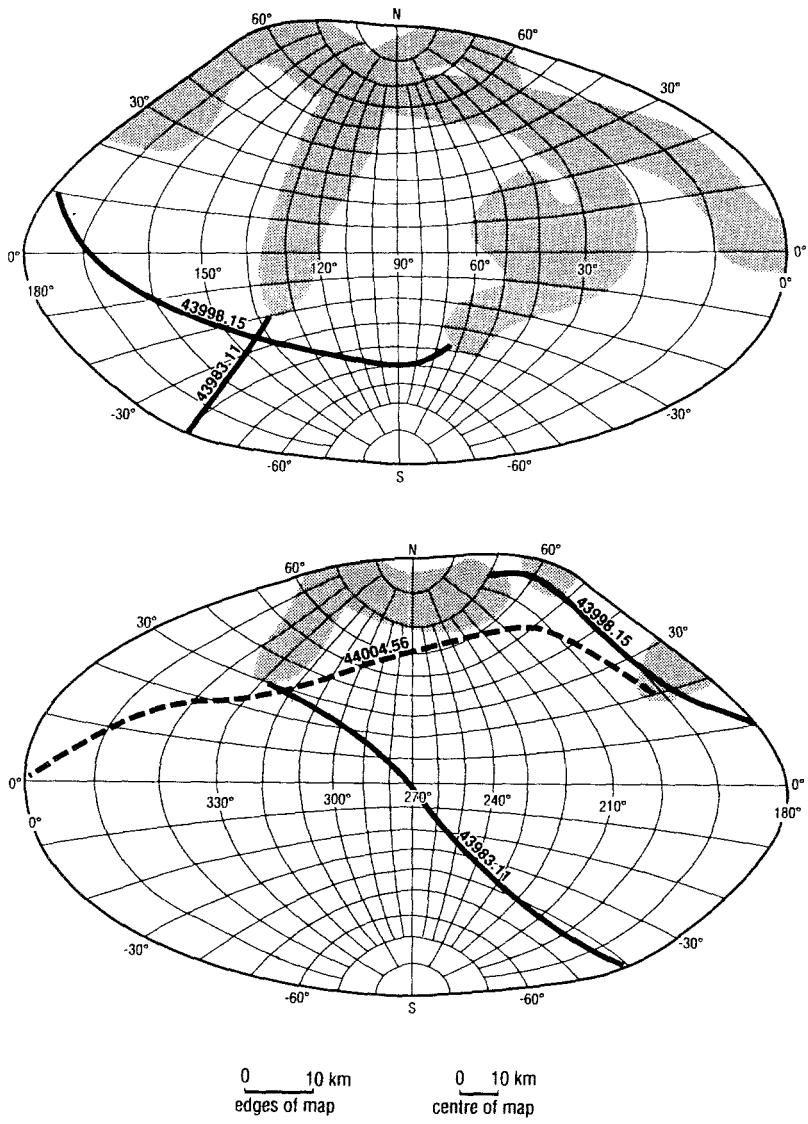

Fig. 1(b).

orientation of the satellite in the original images. Six mutually perpendicular views are presented in Figure 3a, including polar views which show the estimated shape of the equator.

Figure 4 is a shaded relief map of the surface of Prometheus on a Morphographic Conformal projection, a conventional Stereographic projection modified for use with non-spherical objects (Stooke, 1986). The shape used to control the projection

TABLE II

Radii of the Prometheus model (km)

	Longitude									
Lat.	90	80	70	60	50	40	30	20	10	0
90	32.5	32.5	32.5	32.5	32.5	32.5	32.5	32.5	32.5	32.5
80	36.5	36.3	36.1	35.9	35.7	35.5	35.3	35.0	34.8	34.6
70	37.6	36.8	36.4	36.4	36.9	36.9	36.8	35.2	33.7	32.9
60	37.2	35.4	35.0	35.6	36.2	37.0	37.4	35.7	34.4	33.0
50	35.6	34.5	37.2	37.1	37.0	36.9	37.9	36.9	35.8	34.1
40	34.7	35.7	40.1	40.3	39.9	39.7	40.0	40.0	39.0	38.7
30	36.7	38.8	43.1	44.0	43.8	43.8	44.5	45.0	46.1	47.6
20	39.3	44.0	46.5	47.9	49.5	51.4	51.0	50.5	57.2	63.5
10	43.0	46.6	50.2	52.9	55.3	57.4	54.9	53.8	60.7	73.7
0	42.2	46.9	50.0	53.1	56.3	60.2	61.8	61.8	68.2	75.0
−10	39.9	43.5	47.3	50.9	54.1	58.9	62.5	64.8	68.0	69.5
−20	36.2	39.1	41.1	43.4	47.1	51.9	54.7	54.7	56.1	59.2
−30	34.3	35.3	36.7	38.1	40.5	44.4	46.6	47.3	47.8	49.8
−40	31.6	32.2	32.9	34.4	36.2	39.5	40.8	41.4	42.0	42.4
−50	30.5	30.9	31.4	32.4	33.4	35.6	37.0	37.2	37.5	37.5
−60	30.5	31.1	31.3	31.6	32.5	33.5	34.5	34.6	34.7	34.8
−70	31.1	31.3	31.6	31.8	32.1	32.4	32.6	32.9	33.1	33.3
−80	31.0	31.1	31.2	31.3	31.5	31.6	31.7	31.8	31.9	32.0
−90	31.5	31.5	31.5	31.5	31.5	31.5	31.5	31.5	31.5	31.5

	Longitude									
Lat.	180	170	160	150	140	130	120	110	100	90
90	32.5	32.5	32.5	32.5	32.5	32.5	32.5	32.5	32.5	32.5
80	36.4	36.5	36.7	36.8	36.9	36.9	36.8	36.7	36.6	36.5
70	39.0	39.1	39.2	39.2	38.8	38.8	38.7	38.6	38.4	37.6
60	42.5	41.9	41.0	40.5	39.9	39.4	39.5	39.3	38.8	37.2
50	42.0	41.3	40.0	38.5	37.5	37.5	38.1	39.0	38.7	35.6
40	42.4	39.9	38.9	37.0	36.3	36.7	37.6	37.8	38.2	34.7
30	43.4	41.3	39.3	37.7	37.5	38.0	39.7	39.4	39.4	36.7
20	47.7	45.6	45.5	43.4	42.4	42.2	42.9	42.7	41.7	39.3
10	60.6	56.5	55.3	53.7	50.8	47.9	46.7	46.5	44.8	43.0
0	73.5	67.5	62.8	59.1	53.4	49.9	47.9	47.3	45.7	42.2
−10	71.5	65.4	58.0	54.9	49.2	45.9	44.3	43.0	41.5	39.9
−20	59.2	56.7	52.3	48.0	44.0	41.9	39.3	37.2	36.5	36.2
−30	47.4	46.6	44.8	42.5	39.8	37.6	35.2	33.3	32.7	34.3
−40	41.5	40.4	38.9	37.8	36.5	34.5	32.7	31.2	30.9	31.6
−50	36.9	36.5	35.8	35.0	34.0	32.9	31.9	31.3	30.8	30.5
−60	34.1	33.8	33.5	33.0	32.5	31.9	31.4	31.0	30.7	31.1
−70	32.5	32.4	32.2	32.1	31.9	31.7	31.5	31.4	31.2	31.1
−80	31.6	31.5	31.5	31.4	31.3	31.3	31.2	31.1	31.1	31.0
−90	31.5	31.5	31.5	31.5	31.5	31.5	31.5	31.5	31.5	31.5

is the three dimensional convex hull of the model, a refinement of this mapping procedure designed to reduce distortion (Stooke, 1992b). The outline of each map is the convex hull of the satellite in the plane containing the long and short (rotation) axes. In Figure 5 the shaded relief drawing has radius contours superimposed. Radii are given in kilometres with a contour interval of 5 km. Elevations

TABLE II. Continued

	Longitude									
Lat.	270	260	250	240	230	220	210	200	190	180
90	32.5	32.5	32.5	32.5	32.5	32.5	32.5	32.5	32.5	32.5
80	32.7	32.9	33.2	33.6	34.0	34.6	35.1	35.7	36.1	36.4
70	32.3	32.5	32.4	32.5	33.3	33.4	34.1	35.3	37.4	39.0
60	29.9	29.4	30.2	32.1	34.6	35.9	36.5	36.3	39.7	42.5
50	31.3	30.2	30.8	32.5	35.5	39.8	42.2	41.8	41.8	42.0
40	34.1	34.1	35.1	36.0	39.3	43.5	47.6	49.2	45.3	42.4
30	37.4	38.5	40.6	42.6	44.8	47.3	48.1	48.9	48.3	43.4
20	38.1	42.4	44.4	46.7	51.2	53.1	53.5	53.7	50.9	47.7
10	40.6	44.8	46.9	49.5	53.7	58.7	60.4	61.7	65.4	60.6
0	44.7	46.0	47.8	51.7	52.8	63.2	66.4	64.8	71.7	73.5
−10	44.0	45.2	46.8	47.9	49.8	56.0	61.6	64.3	69.4	71.5
−20	42.8	43.5	45.2	45.4	46.1	46.6	46.8	51.6	54.9	59.2
−30	38.4	37.2	38.0	39.8	41.1	41.6	41.8	44.6	46.1	47.4
−40	34.8	33.7	34.2	35.2	36.4	37.4	38.7	39.9	40.9	41.5
−50	32.0	32.3	32.8	33.4	34.2	35.1	35.9	36.4	36.8	36.9
−60	31.5	31.7	32.0	32.3	32.7	33.1	33.6	33.8	34.0	34.1
−70	31.7	31.7	31.8	31.8	32.0	32.1	32.2	32.3	32.4	32.5
−80	31.3	31.3	31.3	31.3	31.4	31.4	31.5	31.5	31.5	31.6
−90	31.5	31.5	31.5	31.5	31.5	31.5	31.5	31.5	31.5	31.5

	Longitude									
Lat.	360	350	340	330	320	310	300	290	280	270
90	32.5	32.5	32.5	32.5	32.5	32.5	32.5	32.5	32.5	32.5
80	34.6	34.4	34.1	33.7	33.3	33.0	32.8	32.6	32.6	32.7
70	32.9	32.9	33.1	33.6	33.0	32.1	31.1	31.5	32.0	32.3
60	33.0	32.2	33.4	34.1	32.9	30.6	29.2	29.8	30.0	29.9
50	34.1	34.1	35.4	34.6	32.9	32.1	28.4	29.8	31.7	31.3
40	38.7	40.3	39.1	36.7	34.8	33.6	32.4	32.1	32.8	34.1
30	47.6	46.2	43.1	41.4	38.7	36.9	35.3	34.5	35.5	37.4
20	63.5	53.7	51.9	48.0	44.2	41.3	38.6	35.4	35.0	38.1
10	73.7	66.1	60.5	53.3	45.5	45.6	40.3	39.2	39.8	40.6
0	75.0	70.0	64.5	55.5	49.2	48.9	46.4	44.9	44.1	44.7
−10	69.5	66.4	61.9	56.6	51.5	48.0	45.5	44.0	43.2	44.0
−20	59.2	57.4	56.2	49.2	48.4	47.7	45.2	43.3	42.1	42.8
−30	49.8	48.6	46.3	42.1	41.7	40.8	40.2	40.1	40.6	38.4
−40	42.4	41.8	40.7	38.3	37.9	37.1	36.6	35.4	34.6	34.8
−50	37.5	37.1	36.5	35.8	35.0	34.3	33.5	32.9	32.4	32.0
−60	34.8	34.6	34.2	33.8	33.3	32.9	32.5	32.1	31.8	31.5
−70	33.3	33.2	33.0	32.8	32.6	32.3	32.1	31.9	31.8	31.7
−80	32.0	31.9	31.8	31.8	31.7	31.6	31.5	31.4	31.3	31.3
−90	31.5	31.5	31.5	31.5	31.5	31.5	31.5	31.5	31.5	31.5

relative to the original 140 by 100 by 75 km triaxial ellipsoid are superimposed on relief in Figure 6.

Prometheus is extremely elongated, as clearly seen in Figures 2 and 3. The equatorial outline resembles a battered rectangle more than an ellipse. The south polar region, which is nowhere observed in the images, is portrayed as smooth and symmetrical. While it is presumably less regular in reality, large protrusions in mid-southern latitudes would certainly be visible in the images, though major

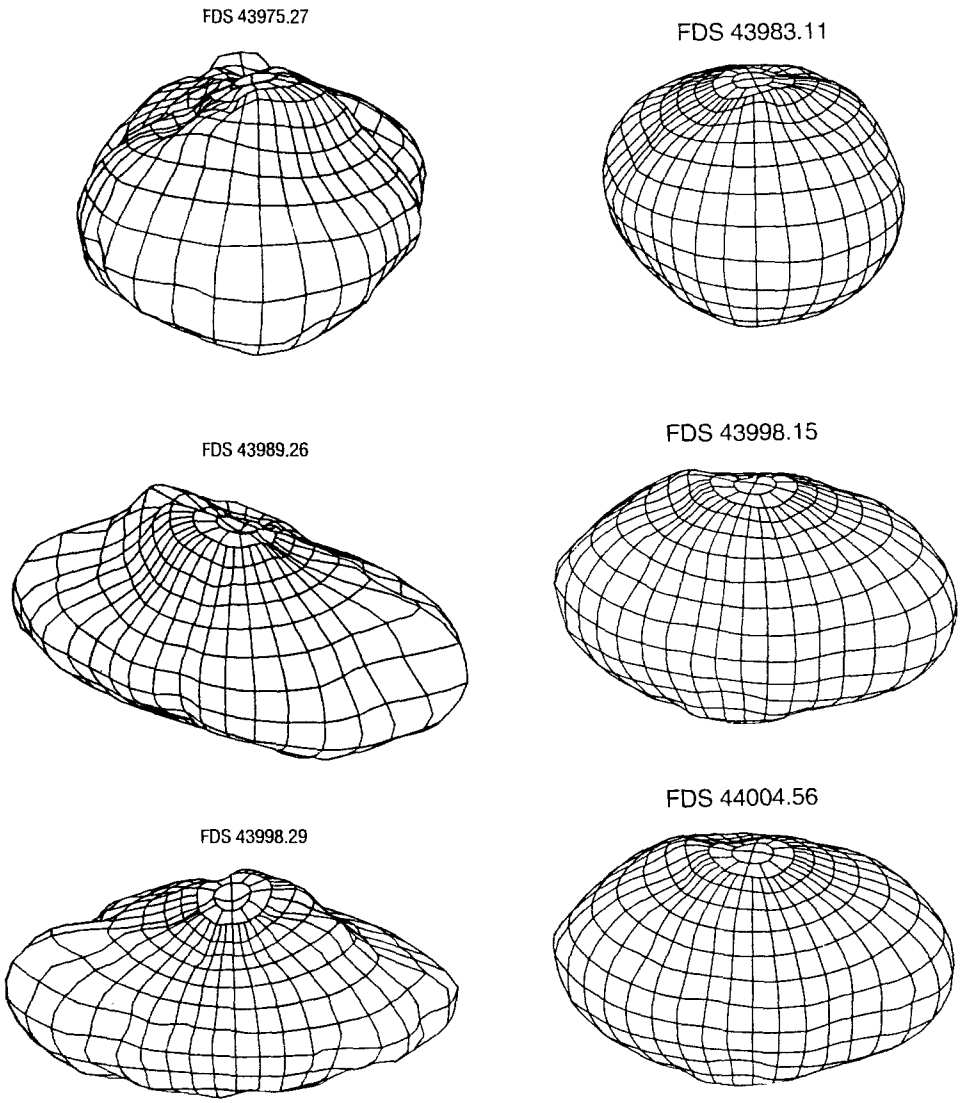

Fig. 2. Latitude-longitude grids in orthographic projection corresponding to three Voyager images of Prometheus (left) and Pandora (right). See Table I for further details.

concavities in the far south would remain undetected. The view along the long axis is irregular but fairly symmetrical.

The maximum radius in the model is 75 km at the sub-Saturn point (0° N, 0° W). The minimum radius is 28.4 km at 50° N, 300° W, though in this region the radii are weakly constrained. The equatorial diameter of the model from 0° to 180° longitude is 148.5 km. From 90° to 270° the equatorial diameter is 86.9 km, and the polar diameter of the model is 64 km.

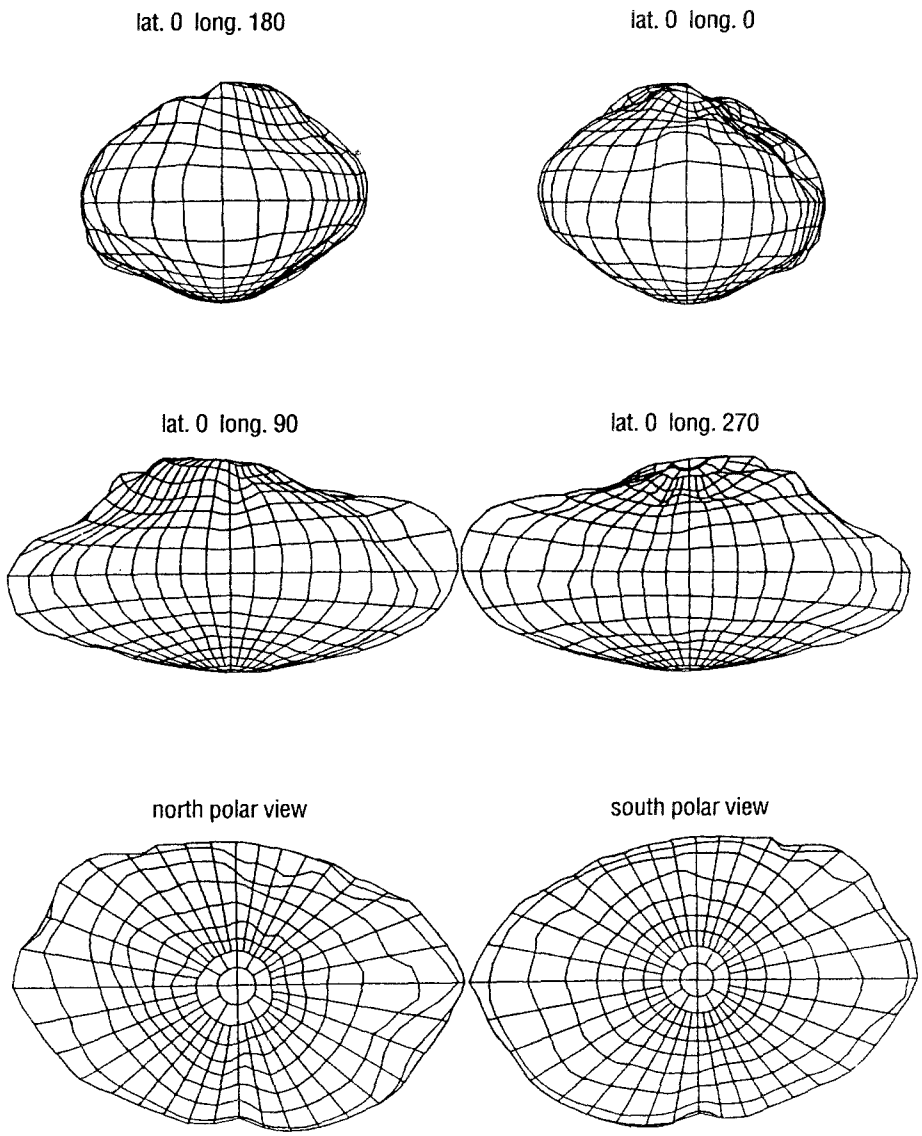

Fig. 3. (a) Orthographic latitude-longitude grids representing Prometheus, viewed from six mutually perpendicular directions. (b) Orthographic latitude-longitude grids representing Pandora, viewed from six mutually perpendicular directions.

The volume of the model is $3.9 \pm 1.0 \times 10^5$ km^3. This is significantly less than the previous estimate of $5.3 \pm 1.0 \times 10^5$ km^3 by Thomas (1989). Thomas's volume was estimated from a triaxial ellipsoid with dimensions of 148, 100 and 68 km, slightly different from the earlier ellipsoidal model (Thomas *et al.*, 1983) adopted as the starting point for this analysis. The difference results mainly from the smaller value for the intermediate axis derived here, and to a lesser extent from

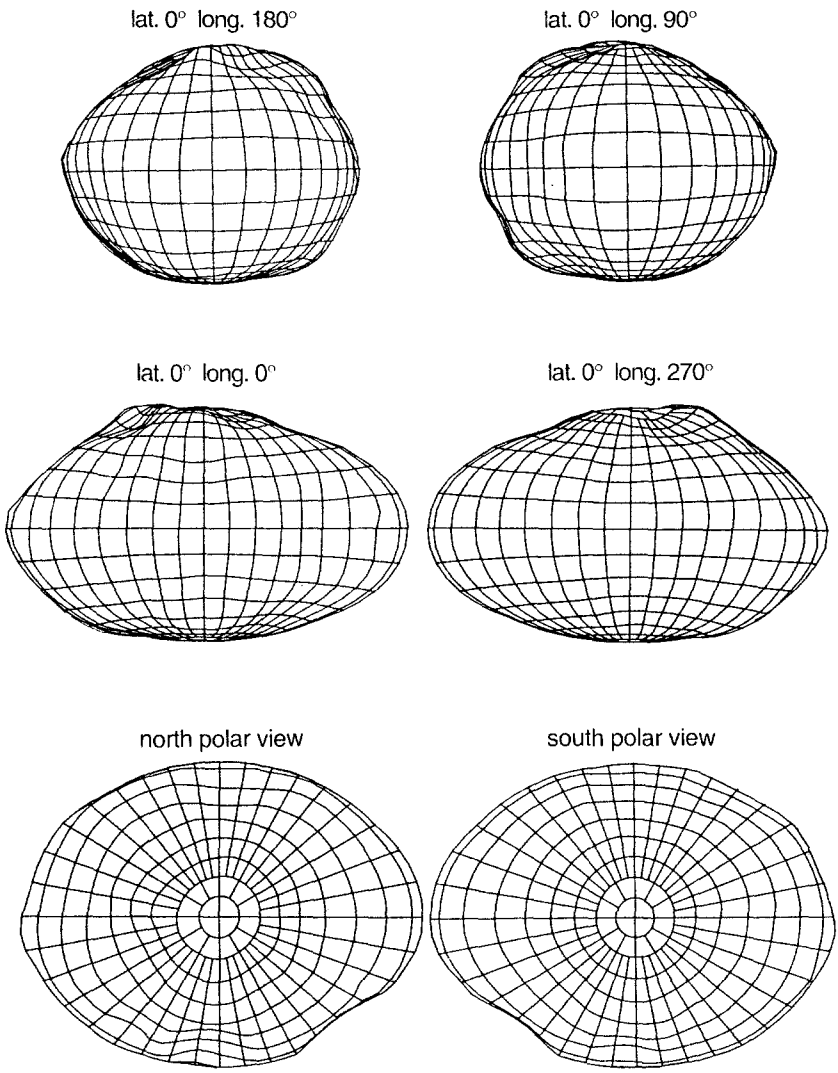

Fig. 3(b).

the incorporation of large depressions and craters. If a triaxial ellipsoid model is required, axes of 145, 85 and 60 km give a better estimate of overall shape and volume.

Assuming the same density of about $0.7\,\mathrm{g\,cm^{-3}}$ estimated for Epimetheus (Stooke, 1993), this volume leads to a mass estimate of $2.7 \pm 1.0 \times 10^{20}$ g. Previous mass estimates, made for the purpose of modelling the dynamics of the F Ring, are considerably larger. Showalter and Burns (1982) assumed a density of $1.2\,\mathrm{g\,cm^{-3}}$ and the volume of a 140 by 100 by 75 km ellipsoid (Thomas *et al.*,

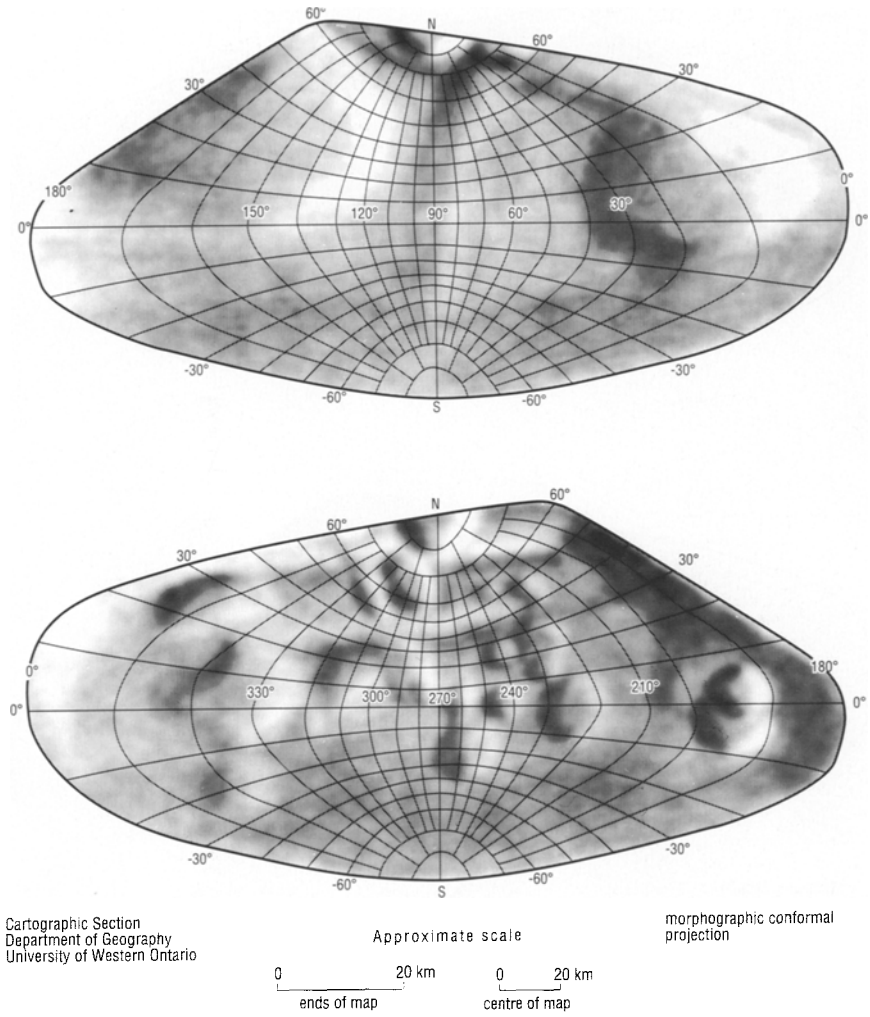

Fig. 4. Shaded relief map of Prometheus on the Morphographic Conformal Projection.

1983) to estimate the mass of Prometheus at $6.6 \pm 3.3 \times 10^{20}$ g. Lissauer and Peale (1986) assumed a density of $1.0\,\mathrm{g\,cm^{-3}}$ and the same volume to obtain a mass estimate of 5.7×10^{20} g. The low density of $0.7\,\mathrm{g\,cm^{-3}}$ adopted here is open to question, but at least a significant part of the lower mass is due to the considerably smaller volume assigned to Prometheus. In future dynamical studies of the F Ring, a smaller mass should probably be adopted for Prometheus.

Thomas *et al.* (1983) noted that 'A prominent linear ridge about 100 km in length traverses the 0–180° longitude on the northern side of the Inner F Ring Shepherd . . . . Seen from the anti-Saturn side (180° longitude), this satellite is

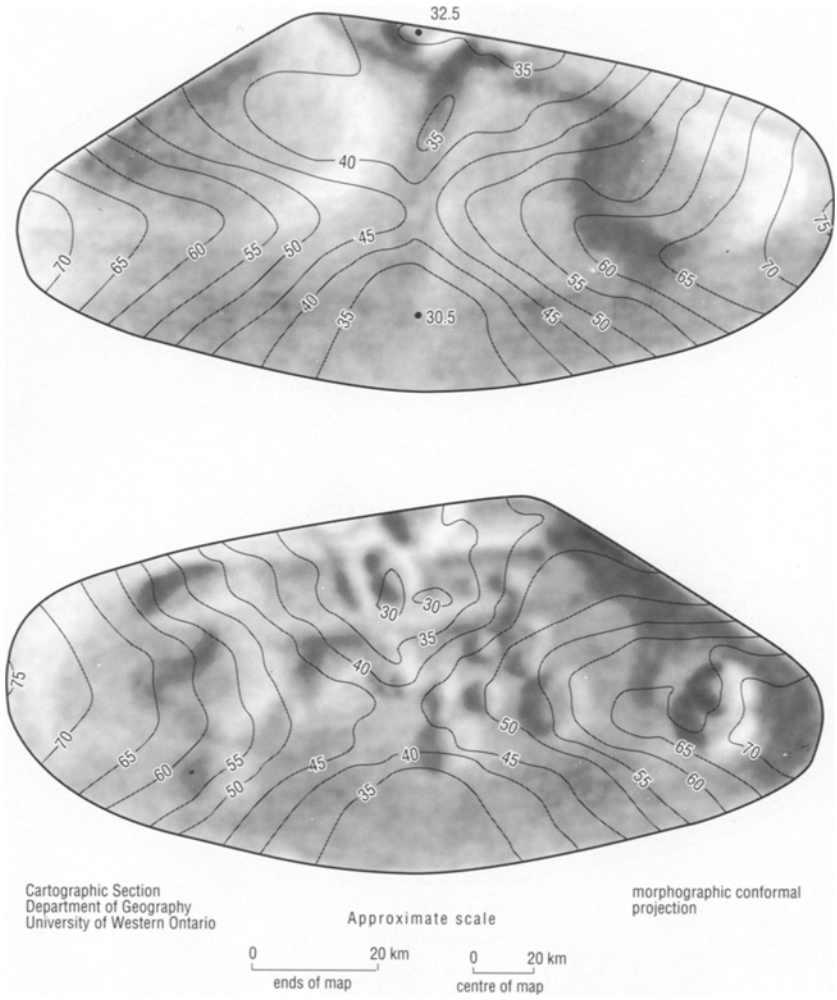

Fig. 5. Shaded relief map of Prometheus with contours of local radius in kilometres at 5 km intervals.

very irregular, but it is not clear how the ridge is related to this cross-section of the satellite'. The transit images have such low resolution (11 km/pixel) that even the least smeared frame contributes very little to the model apart from confirming a roughly equidimensional shape in that orientation. Nevertheless, the transit images reveal a significant topographic irregularity in the region near the anti-Saturn point. Shading on the disk, assumed here to be caused solely by surface slope, suggests that a considerable depression exists north of the equator near longitude 160°, and that the equator itself lies on a prominent ridge (Figure 2, top left). The depression is drawn in Figures 4 to 6 as a large crater, some 60 km in diameter. Its presence also helps to account for the shapes of the terminators in

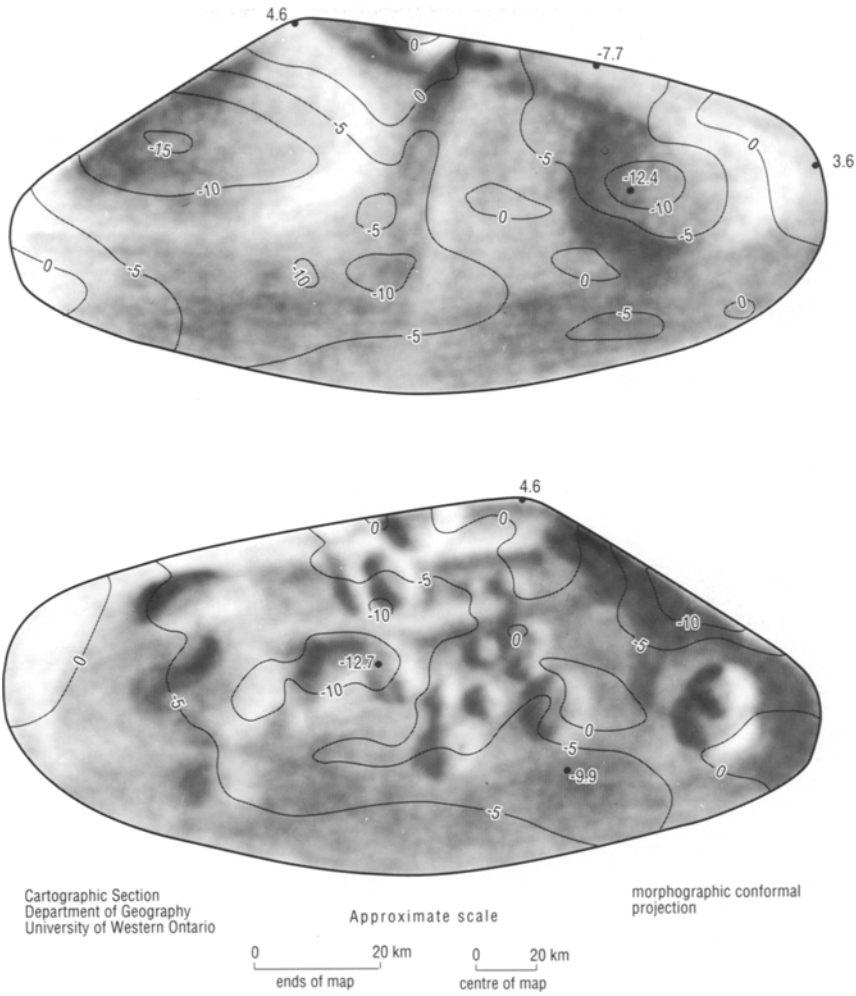

Fig. 6. Shaded relief map of Prometheus with contours of elevation relative to a 140 by 100 by 75 km triaxial ellipsoid. The contour interval is 5 km.

the two higher resolution images. Another possible large crater is faintly seen in image 43989.26 near 10° N, 20° W. Its diameter is roughly 35 km. These features cannot be conclusively identified as impact craters.

The Shape of Pandora

The topographic model of Pandora is presented in Table III and illustrated in Figures 2, 3 and 7 to 9. As for Prometheus, grids corresponding to three Voyager views are given in Figure 2 and six mutually perpendicular views are presented in Figure 3b. Figure 7 is a shaded relief map of the surface of Pandora on a Morpho-

TABLE III

Radii of the Pandora model (km)

	Longitude									
Lat.	90	80	70	60	50	40	30	20	10	0
90	33.5	33.5	33.5	33.5	33.5	33.5	33.5	33.5	33.5	33.5
80	33.6	33.6	33.4	33.3	33.3	33.4	33.5	33.5	33.6	33.7
70	34.6	34.2	33.6	33.3	33.1	33.3	33.6	34.0	34.3	34.4
60	36.7	36.0	34.9	34.2	34.0	34.7	35.5	35.6	35.4	34.8
50	38.5	38.0	36.8	36.1	36.4	37.6	37.3	36.8	36.4	36.2
40	39.4	39.1	38.8	38.5	39.2	39.9	40.6	40.0	39.9	39.8
30	36.8	38.8	39.8	40.6	41.5	42.7	43.8	44.4	45.0	45.3
20	36.8	39.0	41.5	42.5	43.9	45.4	47.2	48.3	50.0	50.6
10	39.1	41.2	42.7	43.9	43.9	44.8	48.0	52.4	54.7	55.6
0	42.0	42.3	43.0	44.3	43.3	44.0	47.8	52.1	56.3	57.7
−10	40.9	41.2	42.4	43.6	43.5	44.4	47.7	52.0	55.1	56.0
−20	38.2	38.4	40.8	42.0	43.3	44.7	46.4	48.7	50.7	51.5
−30	38.8	38.7	40.3	40.8	40.3	40.7	41.9	43.4	45.0	45.6
−40	38.8	38.6	38.5	38.1	37.1	37.3	38.0	39.1	40.3	40.6
−50	36.8	36.6	36.0	35.6	35.0	35.0	35.5	36.2	37.1	37.2
−60	34.1	34.0	33.9	33.7	33.7	34.0	34.2	34.4	34.5	34.6
−70	32.2	32.2	32.3	32.3	32.4	32.5	32.6	32.7	32.8	32.8
−80	31.6	31.6	31.6	31.7	31.7	31.7	31.8	31.8	31.8	31.8
−90	31.5	31.5	31.5	31.5	31.5	31.5	31.5	31.5	31.5	31.5

	Longitude									
Lat.	180	170	160	150	140	130	120	110	100	90
90	33.5	33.5	33.5	33.5	33.5	33.5	33.5	33.5	33.5	33.5
80	33.8	33.8	33.8	33.7	33.7	33.7	33.7	33.6	33.6	33.6
70	35.9	36.4	36.6	36.3	36.1	35.5	35.1	34.9	34.8	34.6
60	38.9	37.0	36.2	36.0	36.6	36.9	36.9	37.0	37.1	36.7
50	39.1	37.5	36.1	35.8	36.3	37.4	38.2	38.5	38.5	38.5
40	40.3	40.1	39.7	39.3	39.1	39.8	39.8	39.9	39.7	39.4
30	43.2	44.1	44.5	43.9	42.8	40.8	40.5	39.7	37.1	36.8
20	47.3	48.2	48.4	47.2	45.2	41.7	42.2	39.7	37.0	36.8
10	52.0	52.6	51.7	49.8	47.7	45.6	44.0	42.0	38.4	39.1
0	56.0	55.8	52.8	50.7	48.4	46.7	44.5	43.1	41.3	42.0
−10	53.7	53.2	52.9	49.9	47.8	46.1	43.7	42.4	41.7	40.9
−20	49.6	49.4	48.7	47.7	45.7	43.9	42.2	40.9	40.2	38.2
−30	45.6	45.1	44.7	43.8	42.7	41.8	40.2	39.9	39.8	38.8
−40	42.0	41.7	41.4	40.2	39.6	39.0	38.4	39.2	39.0	38.8
−50	38.1	37.3	37.2	37.0	36.5	36.0	35.7	36.0	36.6	36.8
−60	34.7	34.6	34.5	34.2	34.0	33.8	33.7	33.9	34.0	34.1
−70	32.9	32.9	32.8	32.7	32.6	32.5	32.4	32.3	32.2	32.2
−80	31.9	31.8	31.8	31.8	31.7	31.7	31.7	31.7	31.6	31.6
−90	31.5	31.5	31.5	31.5	31.5	31.5	31.5	31.5	31.5	31.5

graphic Conformal projection. Again the three dimensional convex hull of the model is the basis for the projection. In Figure 8 the shaded relief drawing has radius contours superimposed, and elevations relative to the original 110 by 85 by 65 km triaxial ellipsoid are plotted in Figure 9.

Pandora is less elongated than Prometheus, as clearly seen in Figures 2 and 3. The equatorial outline is roughly elliptical with a large indentation near longitude

TABLE III. Continued

	Longitude									
Lat.	270	260	250	240	230	220	210	200	190	180
90	33.5	33.5	33.5	33.5	33.5	33.5	33.5	33.5	33.5	33.5
80	33.3	33.1	33.0	33.0	33.0	33.1	33.2	33.4	33.6	33.8
70	33.0	32.6	32.3	32.2	32.4	33.1	33.8	34.5	35.2	35.9
60	32.8	32.6	32.1	32.1	32.4	33.7	35.2	37.1	38.8	38.9
50	33.9	33.9	33.4	33.4	34.0	35.1	37.0	38.3	39.6	39.1
40	35.1	35.5	36.1	36.3	37.2	38.5	39.3	40.5	41.0	40.3
30	35.4	36.5	38.4	39.5	40.8	42.1	42.4	42.4	42.6	43.2
20	37.8	39.0	41.3	42.6	44.1	45.6	46.1	46.1	46.5	47.3
10	41.5	42.2	43.4	44.6	46.4	48.3	49.4	50.1	50.8	52.0
0	42.4	42.5	43.5	44.4	45.5	48.1	51.2	52.7	53.9	56.0
−10	40.6	40.8	41.6	42.1	44.0	46.5	49.9	51.7	53.0	53.7
−20	38.9	39.0	39.7	40.1	42.2	44.5	47.0	48.4	49.3	49.6
−30	37.1	37.1	37.7	38.7	40.8	42.3	44.0	45.6	46.1	45.6
−40	35.4	35.4	35.8	36.8	38.4	39.4	41.1	42.2	42.6	42.0
−50	34.6	34.5	34.9	35.7	36.1	36.5	37.7	38.4	38.6	38.1
−60	33.7	33.8	33.9	34.0	34.2	34.3	34.5	34.6	34.7	34.7
−70	32.6	32.6	32.6	32.7	32.7	32.8	32.9	32.9	32.9	32.9
−80	31.8	31.8	31.8	31.8	31.8	31.9	31.9	31.9	31.9	31.9
−90	31.5	31.5	31.5	31.5	31.5	31.5	31.5	31.5	31.5	31.5

	Longitude									
Lat.	360	350	340	330	320	310	300	290	280	270
90	33.5	33.5	33.5	33.5	33.5	33.5	33.5	33.5	33.5	33.5
80	33.7	33.7	33.8	33.8	33.8	33.8	33.7	33.6	33.5	33.3
70	34.4	34.5	34.6	34.6	34.3	34.0	33.9	33.8	33.4	33.0
60	34.8	34.7	35.3	35.2	34.7	34.5	34.4	34.0	33.8	32.8
50	36.2	36.2	36.4	36.2	35.9	35.8	35.3	34.6	34.0	33.9
40	39.8	39.6	39.6	39.0	38.1	37.2	36.4	35.5	34.8	35.1
30	45.3	44.6	43.9	43.1	42.5	41.0	39.4	37.9	36.0	35.4
20	50.6	50.2	48.9	47.6	46.1	44.8	42.8	40.0	38.3	37.8
10	55.6	54.9	52.7	50.2	48.2	46.9	45.1	43.2	42.1	41.5
0	57.7	56.9	54.4	51.1	48.9	46.9	45.2	43.5	42.6	42.4
−10	56.0	55.3	53.0	49.8	47.9	46.0	44.5	42.8	41.0	40.6
−20	51.5	50.8	49.0	46.9	45.4	43.9	42.7	41.4	39.5	38.9
−30	45.6	45.2	44.1	43.3	42.2	41.2	40.3	39.2	37.6	37.1
−40	40.6	40.6	40.2	39.7	39.1	38.5	37.9	37.4	36.0	35.4
−50	37.2	37.2	37.0	36.8	36.4	36.1	35.7	35.5	35.2	34.6
−60	34.6	34.6	34.6	34.4	34.3	34.1	34.0	33.8	33.8	33.7
−70	32.8	32.9	32.8	32.8	32.8	32.7	32.6	32.6	32.6	32.6
−80	31.8	31.8	31.8	31.8	31.8	31.8	31.8	31.8	31.8	31.8
−90	31.5	31.5	31.5	31.5	31.5	31.5	31.5	31.5	31.5	31.5

40°. The south polar region, which is not visible in the images, is portrayed as smooth and symmetrical. The view along the long axis is irregular but fairly symmetrical.

The maximum radius in the model is 57.7 km at 0° N, 0° W (the sub-Saturn point). The minimum radius is 31.5 km at the south pole. The equatorial diameter of the model from 0° to 180° longitude is 113.7 km. From 90° to 270° the equatorial diameter is 84.4 km, and the polar diameter of the model is 65 km.

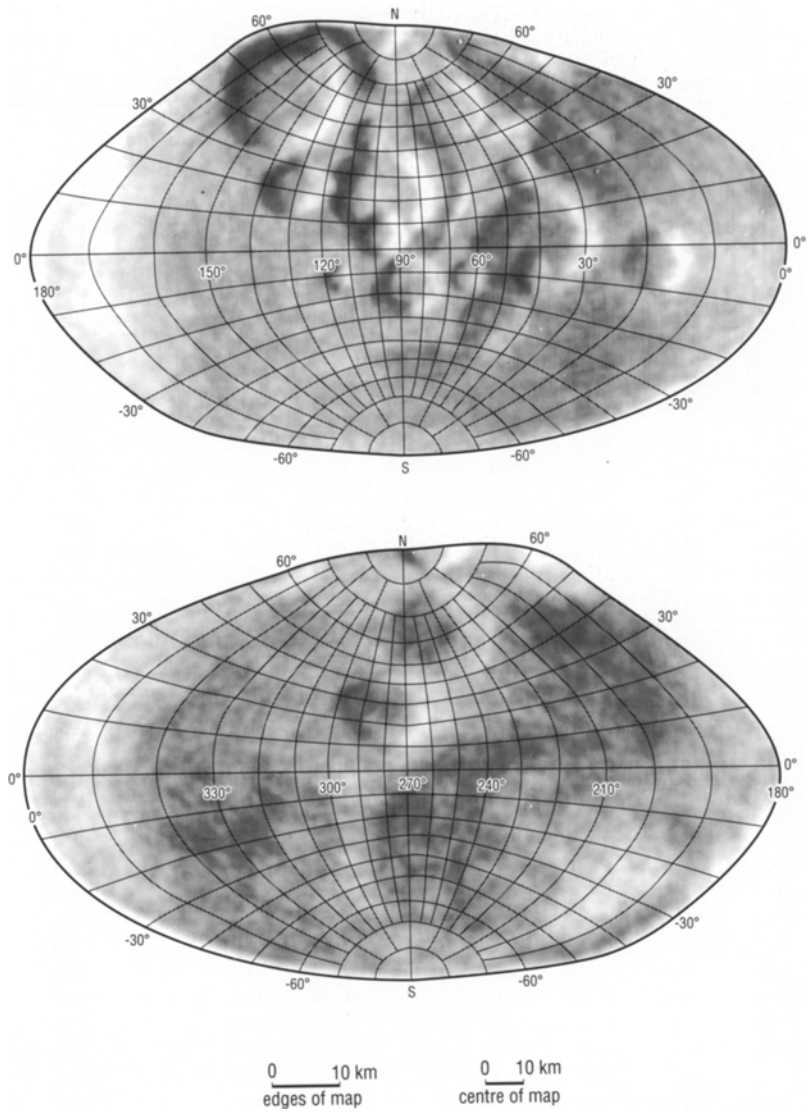

Fig. 7. Shaded relief map of Pandora on the Morphographic Conformal Projection.

The volume of the model is $3.1 \pm 1.0 \times 105\ km^3$, identical to the previous estimate of $3.1 \pm 0.7 \times 10^5\ km^3$ by Thomas (1989), except that a larger uncertainty is considered appropriate here. Although it is likely that positive and negative radius residuals would partly offset each other to reduce the total uncertainty in volume, making Thomas's value quite reasonable, experience with shape modelling tends to favour a more conservative statement of uncertainty. The estimate given by

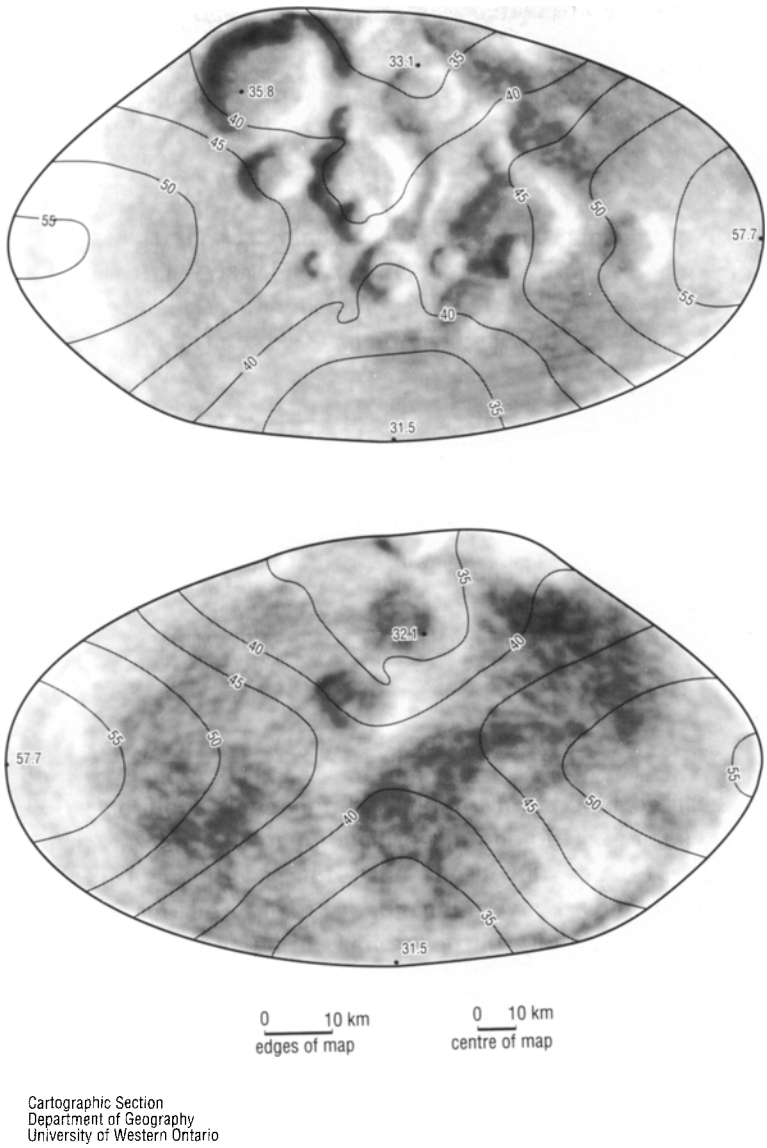

Fig. 8. Shaded relief map of Pandora with contours of local radius in kilometres at 5 km intervals.

Thomas is based on a triaxial ellipsoid with dimensions of 110, 88 and 62 km, slightly different from the earlier ellipsoidal model (Thomas *et al.*, 1983) adopted as the starting point for this analysis. A triaxial ellipsoid with axes of 114, 84 and 62 km gives a better estimate of shape and volume. Assuming the same density of about 0.7 g/cm^3 estimated for Epimetheus (Stooke, 1993), this volume leads to a mass estimate of $2.2 \pm 1.0 \times 10^{20}$ g. As for Prometheus, previous estimates were considerably higher. Showalter and Burns (1982) estimated the mass of Pandora

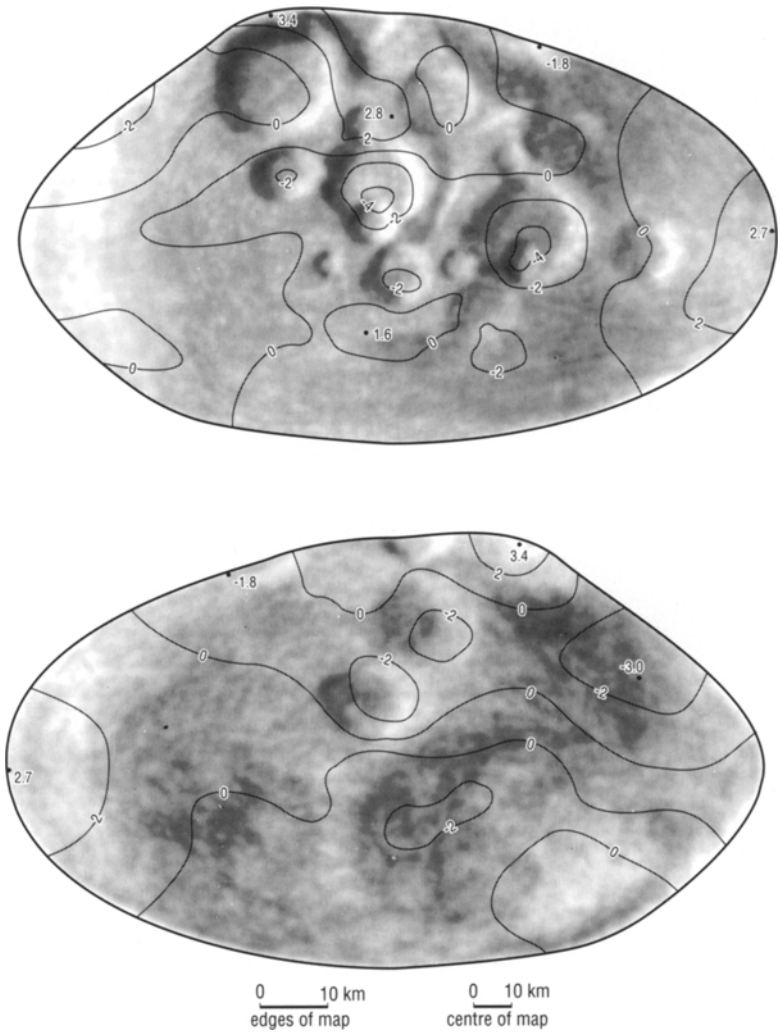

Fig. 9. Shaded relief map of Pandora with contours of elevation relative to a 110 by 85 by 65 km triaxial ellipsoid. The contour interval is 2 km.

as $4 \pm 2 \times 10^{20}$ g, and Lissauer and Peale (1986) estimated 3.4×10^{20} g, based on assumptions similar to those made for Prometheus. Since Pandora is smaller and further from the F Ring, its mass is of lesser significance in studies of the shepherding and braiding processes, but the smaller mass suggested here should probably be considered in detailed dynamical studies.

Image 44004.46 shows the northern limb at high phase angle. No topographic features are obvious within the bright crescent, but two faint extensions to the

crescent deserve mention. One appears to be the southern rim of a 25 km crater at 50° N, 150° W (Figure 7). The other, fainter still, is the Saturn-facing side of the satellite illuminated by light reflected from Saturn itself. The light level is too low to reveal topographic features, with the possible exception of a darker region near the centre of the disk. This is probably the 30 km crater at 20° N, 100° W (Figure 4), forming an indentation in the Saturnshine terminator. If this interpretation is correct the assumption of a synchronous rotation state is considerably strengthened.

Surface Features of Prometheus

The shaded relief drawing shows several prominent craters, as well as the two very large depressions noted above. The largest craters are about 20 km across. There are five well defined craters with diameters in the 15 to 20 km range, and several other possible craters of this size suggested by shading or depressions in the limbs. The less certain craters are drawn less distinctly on the maps. A few craters in the 10 km diameter range are visible. However, small irregular depressions may easily be confused with impact craters near the limit of resolution, a tendency which is exaggerated in the shaded relief drawing, so interpretations must be undertaken with caution. For this reason no attempt is made here to investigate crater densities and estimate surface ages.

Only one image of Prometheus (43998.29) has adequate resolution to reveal small craters. Even near the terminator in the region where small craters ought to be most visible (around 30° N, 220° W) few are clearly seen. The smaller features shown in Figure 4 are very faint and many are uncertain. The impression given by this image is of a fairly smooth surface deficient in craters compared with the nearby small satellites. This conclusion must be regarded as tentative until better images are obtained during the Cassini mission.

Apart from craters, the most prominent topographic features revealed in the Voyager images are a system of ridges and valleys crossing the north polar region (Figure 10). The longest ridge extends about 100 km from 40° N, 210° W to 20° S, 0° W across the trailing side of the satellite. It is obscured by craters near the middle of this length, and may not be a truly continuous ridge. It is flanked on either side by two less clearly seen but apparently parallel ridges, one of which forms much of the terminator in image 43998.29. The heights of these ridges and the depths of the intervening valleys are not usefully constrained by the limited data.

Image 43989.26 shows a very faint dark line near the centre of the disk, running from roughly 10° S, 95° W to 70° N, 70° W, a distance of about 60 km. It appears to extend to or nearly to the terminator. Image 43998.29 shows a possible extension of this line at higher resolution. A curving groove or series of depressions appears to flank a pair of larger (20 km) craters, one of which contains the north pole (Figure 4). The groove or chain of depressions is about 10 km across and its

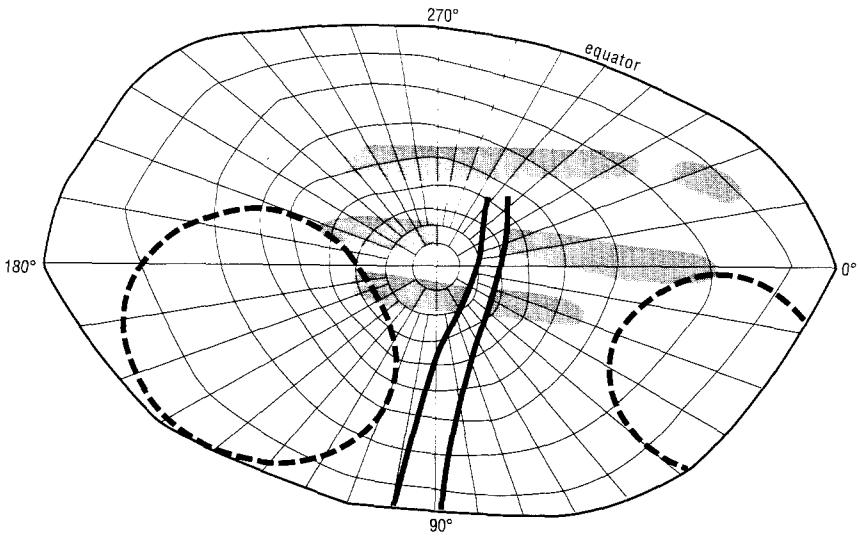

Fig. 10. Major non-crater surface features of Prometheus plotted on an equal area morphographic projection of the satellite's convex hull. The north pole is at the centre and the boundary is the equator. Shading represents prominent ridges. A possible groove or valley is shown as a double line. Rims of two large poorly resolved depressions are represented by dashed curves.

morphology is uncertain. It may be nothing more than a chance arrangement of impact craters. The overall appearance is, however, suggestive of a groove or valley crossing the set of three parallel ridges at right angles to connect with the dark linear feature on the leading side of the satellite (Figure 10). These linear features suggest fairly large scale disruption of the satellite, most likely caused by a catastrophic impact. This disruption may possibly be related to the formation of the F Ring or of the nearby small satellites.

Thomas *et al.* (1986) mention bright markings on Prometheus, suggesting that they may consist of ice less contaminated with darker material than surrounding areas. The two bright patches are centred around 20° N, 250° W and 10° N, 350° W. Topography in each area is difficult to discern because of the high sun angle. The eastern patch appears to be topographically unremarkable and may possibly be explained as ejecta from a relatively recent small crater, perhaps that at 20° N, 240° W (Figure 4). Even on a satellite as small as Prometheus the lowest velocity material ejected near the end of crater excavation should form a localized ejecta blanket, as suggested by apparent ejecta deposits around the crater Stickney on Phobos (Thomas, 1979; Murchie *et al.*, 1991) and around very small craters on asteroid 951 Gaspra recently observed by the Galileo spacecraft (Helfenstein *et al.*, 1992). The western patch of bright material may be associated with steep local slopes near the pointed sub-Saturn end of the satellite or with the ridge at 12° N, 343° W between two large craters. In this case the interpretation would be fresh material exposed by downslope movement, perhaps initiated by impact. The ma-

terial may also be the ejecta of a crater not visible in the image as a result of high sun, low resolution and oblique viewing in this region.

Surface features of Pandora

The surface of Pandora appears to be heavily cratered in image 43998.15. The two largest craters are about 30 km in diameter and the particularly prominent crater at 50° N, 150° W is about 25 km across. It appears larger on the map because of the variation in scale on this (as on any other) conformal map projection. This prominent crater is also faintly but certainly visible in the low resolution multispectral image sequence. There are two certain and three possible craters roughly 15 km across and several possible craters about 10 km across. A few additional craters in the 15 to 20 km size range are suggested by scalloped sections of the terminator, including one at 60° N, 240° W which is invoked to help shape the northern terminator of image 43998.15. The crater depicted at 25° N, 280° W is suggested by very subtle shading in heavily processed versions of image 43983.11, as is a large flattened region about 50 km across at 25° S, 230° W, depicted as a broad shallow depression on the map. All features on the trailing side (centred on 270° W) are extremely speculative because of the very low resolution and small phase angle of the images of that area.

No linear valleys or ridges are visible in the images, with the possible exception of a north-south lineation just east of the large crater at 20° N, 100° W. This is probably nothing more than a combination of the raised rim of that crater and one or two fortuitously placed 10 km craters. Prominent linear ridges like those seen on Prometheus are certainly absent in the 25 per cent of Pandora seen in the best image. The range of elevations revealed in Figure 9 is only ±4 km relative to the ellipsoidal datum, indicating that for purposes of dynamical modelling a simple ellipsoidal model is quite satisfactory. Pandora appears less irregular in shape than its neighbouring satellites in the limited data currently available. No albedo markings are apparent in the images.

Conclusion

Lissauer *et al.* (1985) discuss the orbital acceleration of satellites near the edge of the ring system by ring torque. They assumed a mass for Prometheus of 3.7×10^{20} g and estimated that the ring-induced acceleration would have ejected Prometheus from the A Ring only about 3 million years ago. The co-orbital satellites would have been ejected some 30 to 40 million years ago. The torque is smaller for lower satellite mass, as proposed here, permitting a longer lifetime outside the rings. The effect should be observable in ground-based instruments within a few decades, permitting a dynamical means of estimating the mass of Prometheus which, with the volume estimated here, will give the bulk density of the satellite.

Yoder *et al.* (1989) suggested that the small satellites near the edge of the rings accreted within the rings by low velocity collisions and were expelled to their present locations by ring torque. This would help explain the very low densities proposed by those authors for the co-orbital satellites. The linear features on Prometheus (suggestive of structural continuity rather than a rubble pile interior) and the heavily cratered surfaces on Pandora, Janus and Epimetheus make this suggestion of unconsolidated internal structures and youthful surfaces appear less likely.

During the Cassini mission it should be possible to obtain images at least as good as the best from Voyager 2 for a number of viewing and illumination conditions. With such images the global crater distribution could be observed, the suggested smoothness of Prometheus could be investigated further and the topographic models of each satellite could be substantially improved. Better volumes for the satellites, together with characterizations of their librations and gravitational effects on the F Ring and each other, would lead to better values for their bulk densities and a clearer understanding of the origins of the small inner satellites and the shepherding of planetary rings.

Acknowledgements

The images used for this study were provided courtesy of the National Space Science Data Center, NASA's Planetary Data System and Dr. B. A. Smith, leader of the Voyager Imaging Team. John Pimental helped prepare a preliminary model of Prometheus which contributed to my development and interpretation of the shape described here. I thank Diane Shillington for help with the manuscript, Matthew Lumsdon for assisting with some of the figures, and Gordon Shields for valued cartographic support.

References

Helfenstein, P., Veverka, J., Thomas, P. C., Simonelli, D. P., Carcich, B., McEwan, A. S., Head, J. W., Murchie, S., Chapman, C., Belton, M., Klassen, K. and Fanale, F.: 1992, *Lunar Planet. Sci.* **XXIII**, 519–520.

Lissauer, J. J., Goldreich, P. and Tremaine, S.: 1985, *Icarus* **64**, 425–434.

Lissauer, J. J. and Peale, S. J.: 1986, *Icarus* **67**, 358–374.

Murchie, S. L., Britt, D. T., Head, J. W., Pratt, S. F., Fisher, P. C., Zhukov, B. S., Kuzmin, A. A., Ksanfomality, L. V., Zharkov, A. V., Nikitin, G. E., Fanale, F. P., Blaney, D. L., Bell, J. F. and Robinson, M. S.: 1991, *J. Geophys. Res.* **96**, 5925–5945.

Showalter, M. R. and Burns, J. A.: 1982, *Icarus* **52**, 526–544.

Smith, B. A., Soderblom, L., Beebe, R., Boyce, J., Briggs, G., Bunker, A., Collins, S. A., Hansen, C. J., Johnson, T. V., Mitchell, J. L., Terrile, R. J., Carr, M., Cook, A. F., Cuzzi, J., Pollack, J. B., Danielson, G. E., Ingersoll, A., Davies, M. E., Hunt, G. E., Masursky, H., Shoemaker, E., Morrison, D., Owen, T., Sagan, C., Veverka, J., Strom, R. and Suomi, V. E.: 1981, *Science* **212**, 163–191.

Smith, B. A., Soderblom, L., Batson, R. M., Bridges, P., Inge, J., Masursky, H., Shoemaker, E., Beebe, R., Boyce, J., Briggs, G., Bunker, A., Collins, S. A., Hansen, C. J., Johnson, T. V.,

Mitchell, J. L., Terrile, R. J., Cook, A. F., Cuzzi, J., Pollack, J. B., Danielson, G. E., Ingersoll, A. P., Davies, M. E., Hunt, G., Morrison, D., Owen, T., Sagan, C., Veverka, J., Strom, R. and Suomi, V. E.: 1982, *Science* **215**, 504–537.

Stooke, P. J.: 1986, Proceedings Second International Symposium Spatial Data Handling, Seattle, July, 1986, pp. 523–536.

Stooke, P. J.: 1988, PhD dissertation, University of Victoria, 169 pp.

Stooke, P. J.: 1992a, *Earth, Moon and Planets* **56**, 123–139.

Stooke, P. J.: 1992b, Proceedings, Asteroids, Comets, Meteorites (in press).

Stooke, P. J.: 1993, *Earth Moon and Planets* (in press).

Stooke, P. J. and Abergel, A.: 1991, *Astron. Astrophys.* **248**, 656–688.

Stooke, P. J. and Keller, C. P.: 1990, *Cartographica* **27**, 82–100.

Thomas, P.: 1979, *Icarus* **40**, 223–243.

Thomas, P., Veverka, J., Morrison, D., Davies, M. and Johnson, T. V.: 1983, *J. Geophys. Res.* **88**, 8743–8754.

Thomas, P., Veverka, J. and S. Dermott: 1986, *Satellites*, University of Arizona Press, Tucson, Chap. 17, pp. 802–835.

Thomas, P. C.: 1989, *Icarus* **77**, 248–274.

Yoder, C. F., Synnott, S. P. and Salo, H.: 1989, *Astron. J.* **98**, 1875–1889.